ATMOSPHERIC SCIENCE LETTERS
Atmos. Sci. Let. **17**: 315–325 (2016)
Published online 27 April 2016 in Wiley Online Library
(wileyonlinelibrary.com) **DOI:** 10.1002/asl.660

RMetS
Royal Meteorological Society

On the link between cold fronts and hail in Switzerland

Sebastian Schemm,[1,2,3]* Luca Nisi,[2,3,4] Andrey Martinov,[2,3,4] Daniel Leuenberger[5] and Olivia Martius[2,3,4]

[1]*Geophysical Institute and Bjerknes Centre for Climate Research, University of Bergen, Bergen, Norway*
[2]*Institute of Geography, University of Bern, Bern, Switzerland*
[3]*Oeschger Centre for Climate Change Research, University of Bern, Bern, Switzerland*
[4]*Mobiliar Lab for Natural Risks, University of Bern, Bern, Switzerland*
[5]*Federal Office of Meteorology and Climatology MeteoSwiss, Zurich, Switzerland*

*Correspondence to:
S. Schemm, Geophysical Institute and Bjerknes Centre for Climate Research, University of Bergen, NO-5020 Bergen, Norway.
E-mail:
sebastian.schemm@uib.no

Received: 24 November 2015
Revised: 11 March 2016
Accepted: 18 March 2016

Abstract

Hail is the costliest atmospheric hazard in Switzerland, causing substantial damage to agriculture, cars and buildings every year. In this study, a 12-year statistic of objectively identified cold fronts and a radar-based hail statistic are combined to investigate the co-occurrence of cold fronts and hail in Switzerland. In a first step, an automated front identification scheme, which has previously been designed for and applied to global reanalysis data, is modified for a high-resolution regional analysis data set. This front detection method is then adapted, tested and applied to the Consortium for Small Scale Modelling (COSMO) analysis data for the extended hail season (May to September) in the years 2002–2013. The resulting cold front statistic is presented and discussed. In a second step, the frequency of cold fronts is linked to a high-resolution radar-based hail statistic to determine the relative fraction of hail initiation events in pre-frontal environments. Up to 45% of all detected hail events in north-eastern and southern Switzerland form in pre-frontal zones. Similar fractions are identified upstream of the Jura and the Black Forest mountains. The percentage of front-related hail formation is highest in regions where hail is statistically less frequent, with the exception of southern Switzerland. Furthermore, it is shown that fronts create wind-sheared environments, which are favourable for hail cells.

Keywords: **hail; front; climatology; thunderstorm; high impact weather; severe weather**

1. Introduction

Hail-producing thunderstorms are a frequent natural hazard in Switzerland during the summer months and pose a challenge to numerical weather models and forecasters. Many hail storms are accompanied by large-scale weather fronts but the precise number of pre-frontal hail storms and its regional variability is unknown. In this study, we use a high-resolution regional analysis to quantify the pre-frontal hail fraction of a 12-year radar-observed hail statistic over Switzerland for the 'extended hail season' May to September (Nisi *et al.*, 2016). Recent studies focused on hail occurrence over central Europe (Suwala and Bednorz, 2013; Punge *et al.*, 2014) but yet the number of pre-frontal hail events has not been quantified.

Research on the ambient state of the atmosphere that is favourable for the formation of severe thunderstorms that can produce hail, convective wind gusts or tornadoes has a long tradition, e.g. Fawbush and Miller (1954); Houze *et* al. (1993); Willemse (1995); Schiesser *et al.* (1997); Huntrieser *et al.* (1997); Rasmussen and Blanchard (1998); Brooks *et al.* (2003); Groenemeijer and Delden (2007); Naylor and Gilmore (2012); Grams *et al.* (2012); Manzato (2012); Mohr and Kunz (2013); Gensini *et al.* (2014); Allen and Karoly (2014); Merino *et al.* (2014). Such studies often involve the analysis of proximity-soundings, i.e. soundings obtained in close spatial and temporal proximity to such an event. Proximity soundings allow for the identification of the ambient conditions conducive to the development of severe thunderstorms (Brooks, 2009). These include high values of convective available potential energy (CAPE; Groenemeijer and Delden, 2007), low convective inhibition (CIN; Davies, 2004) and strong vertical wind shear between approximately 0–6 km (Weisman and Klemp, 1982; Doswell and Evans, 2003; Kaltenboeck and Steinheimer, 2015). Also important are a reduced mid-tropospheric lapse rate, a high mixing ratio and high storm relative helicity (Droegemeier *et al.*, 1993). A variety of derived indices, e.g. the significant hail parameter (SHIP) (details are provided at http://www.spc.noaa.gov/sfctest/help/help_sigh.html) or the SWISS index (Huntrieser *et al.*, 1997), have been developed based on empirically or statistically derived combinations of the above-mentioned quantities and others (Manzato, 2013). However, proximity soundings are only representative for the state of the lower troposphere in close vicinity (50–100 km; Haklander and Delden, 2003) to the measurement site and can only provide limited information about the synoptic-scale setting.

The synoptic-scale flow situation can be studied using surface weather charts, radar information, satellite data and analysis data (Towery and Changnon, 1970; Doswell, 1987). Indeed, the role of synoptic-scale

forcing and especially of cold-fronts is important for hail storms, as early investigations of radar data have demonstrated. Studies such as Towery and Changnon (1970) showed that hail cells associated with fronts live longer and move faster, and that a substantial number of hail cases (more than 50%) are linked to frontal features. In a number of case studies, the role of cold fronts for the initiation and life-cycle of severe convection in North America was discussed in detail (e.g. Ogura and Portis, 1982; Heymsfield and Schotz, 1985; Doswell, 1987; Locatelli *et al.*, 1995; Neiman and Wakimoto, 1999). The role of synoptic-scale forcing is mainly to 'set the scene' for severe convection by contributing to a moistening of the lower troposphere through low-level moisture advection and by reducing existing capping inversions through upper-level cold air advection (Doswell, 1987). In addition, cold fronts are important for (1) the triggering of convection (Ogura and Portis, 1982), (2) the upward advection of moisture by the vertical frontal circulation and the initiation of convection through the vertical circulation (Neiman and Wakimoto, 1999) and (3) the formation of convergence lines that trigger the convection (Heymsfield and Schotz, 1985). Alberoni *et al.* (2000); Costa *et al.* (2001) and Giaiotti *et al.* (2003) discuss the role of synoptic-scale forcing and in particular the role of cold fronts associated with severe convection and hail in Northern Italy. Both Costa *et al.* (2001) and Giaiotti *et al.* (2003) point out the importance of the interaction of the large-scale driven flow with the local orography for the formation of hail-producing thunderstorms. This interaction results in important triggers for convection, namely convergence zones associated with cold fronts and the destabilization by the cold advection aloft.

2. Outline and objectives

In this study, we extend the case studies cited above that focused on a limited number of cases (Ogura and Portis, 1982; Heymsfield and Schotz, 1985; Doswell, 1987; Locatelli *et al.*, 1995; Neiman and Wakimoto, 1999) by investigating a larger sample of hail events (~14 000) that occurred in Switzerland and adjacent regions during the extended hail season between 2002 and 2013. The main objectives of this study are:

1 To apply an automated front recognition algorithm to an analysis data set with high spatial and temporal resolution (Steppler *et al.*, 2003; Jenkner *et al.*, 2010). The front algorithm and radar-based hail detection are discussed in Section 3; the front frequency for Switzerland is presented in Section 4.
2 To link the front data to a radar-based data set of hail initiations, *defined as the time when hail is first detected in a thunderstorm cell by the radar*, and to quantify the fraction of pre-frontal hail formations in different regions of Switzerland (Section 5).
3 To characterize the temporal evolution of the vertical wind shear in pre-frontal zones prior to hail formation (Section 6).

3. Methods

3.1. Front detection

The automated detection algorithm for synoptic-scale fronts in the Consortium for Small Scale Modelling (COSMO) analysis data set is based on the work of Jenkner *et al.* (2010) and Schemm *et al.* (2015) and has been shown to be useful for the automated recognition of synoptic-scale fronts in a global reanalysis (Schemm and Sprenger, 2015; Schemm *et al.*, 2015) and in the high resolution COSMO-7 reanalysis data (Jenkner *et al.*, 2010). In this study, the methodology and specific complications arising from its application to a 2 km data set are outlined. The COSMO analysis data set is operationally produced by Meteo Swiss and encompasses approximately 2°–17°E, 42°–50°N (more details at: http://www.cosmo-model.org/content/tasks/operational/meteoSwiss/). The hourly model output is provided with a 6.6 km grid-spacing until 2007 (COSMO-7) and with a 2.2 km grid-spacing (COSMO-2) since 2007 (Steppler *et al.*, 2003; Jenkner *et al.*, 2010). Because the frequency of large-scale weather fronts in the limited area weather predication COSMO model (which is driven by ECMWF forecast fields) is not affected by the increase in the spatial resolution in 2007, and because we do not make use of more sensitive information such as frontal gradients, we decided to use the full time period 2002–2012.

The identification strategy focuses on the localization of the thermal front parameter (TFP; Hewson, 1998), which is defined as

$$\mathrm{TFP} = -\nabla|\nabla\theta_e| \cdot \frac{\nabla\theta_e}{|\nabla\theta_e|}, \qquad (1)$$

where θ_e denotes the equivalent potential temperature. The parameter describes 'the gradient of the magnitude of the gradient of a thermodynamic scalar quantity (here θ_e), resolved into the direction of the gradient of that quantity' (Renard and Clarke, 1965). In other words, the change in the gradient of θ_e is projected along the normal component of the front (perpendicular to the frontal zone) in order to take the curvature of a front into account. The TFP is used to identify the location of the maximum of $|\nabla\theta_e|$ in narrow zones of strong thermal gradients, which are referred to as frontal zones or frontal areas. After a series of manual tests in the COSMO-2 data, we set the threshold for the frontal zone to $|\nabla\theta_e| > 6\,\mathrm{K}\,(100\,\mathrm{km})^{-1}$ at 700 hPa. Note that previous studies use weaker thresholds, e.g. $4\,\mathrm{K}\,(100\,\mathrm{km})^{-1}$ by Schemm *et al.* (2015), which is primarily due to the lower resolution of the data sets used in their analyses. Inside a frontal zone, the actual front is located where the TFP is zero (see Figure 1). To test the sensitivity of the frontal frequencies to the choice of the minimum frontal length, the frontal frequencies obtained with a minimum length of 300 and 500 km are discussed (Section 4). The TFP in this study is evaluated at 700 hPa, because the traditional altitude of

850 hPa (Hewson, 1998; Berry *et al.*, 2011, and references therein) lies below most of Switzerland's high topography. For further details and technical aspects regarding the implementation, testing and validation of the algorithm, the reader is referred to Schemm *et al.* (2015) and Jenkner *et al.* (2010).

The high-resolution data set used in this study poses some additional challenges compared to the previous application of the front detection algorithm:

- To overcome the large gridpoint-to-gridpoint variability in a high-resolution data set, and to avoid the misidentification of localized noise as fronts, a diffusive smoothing is applied to θ_e using a Laplacian filter (see Jenkner *et al.*, 2010).
- In general, the fronts are very thin lines (where TFP = 0, see also Figure 1); the slightly broader frontal zones ($|\nabla\theta_e| > 6\,\mathrm{K}\ (100\,\mathrm{km})^{-1}$) around the detected fronts are therefore used for the calculation of the frontal frequencies.

Finally, we note that frontal identification strategies based on thermal gradients frequently identify thermal boundaries over the Alps, especially during the late evening, that are formed by Alpine pumping (Weissmann *et al.*, 2005). As we are mainly interested in synoptic-scale fronts, we restrict our study to cold fronts and require all identified fronts to live for at least 3 h. Due to the hourly resolution of the data set, an overlap criterion between consecutive time steps is sufficient to determine the lifetime of every front. No frontal tracking algorithm is required. The front type is determined by defining a wind component v_f perpendicular to the front:

$$v_f = \mathbf{v} \cdot \frac{\nabla \mathrm{TFP}}{|\nabla \mathrm{TFP}|}, \tag{2}$$

This advection criterion allows the scheme to distinguish cold ($v_f > 0$) from warm ($v_f < 0$) fronts (where $\mathbf{v}$ denotes the horizontal wind). The requirements introduced above (i.e. a minimum lifetime of 3 h, limitation to cold fronts and minimum length) remove the majority of thermal fronts induced by Alpine pumping. The introduction of additional criteria to remove thermal fronts, e.g. a minimum advection threshold, the time of detection or the location above the Alpine ridge, did not improve the algorithm.

The main differences between the fronts used in this study and the fronts used by Jenkner *et al.* (2010) are the application of the length criterion, the requisite minimum lifetime and the restriction to cold fronts. In addition, the frontal threshold used in this study is slightly higher due to the increased spatial resolution of the data.

3.1.1. Front detection – an illustrative example

To depict a typical synoptic situation with a cold front and pre-frontal hail formation on the northern side of the Alps, an example from the first of July 2012 at 0600 UTC is presented in Figure 1. The synoptic situation was dominated by a long-wave quasi-stationary trough over the East Atlantic and Western Europe. The Alpine area was located in a warm sector ahead of a cold front that moved eastward across Central Europe. Because of Foehn winds from the south, the northern side of the Alps was initially rather dry. However, a moderate mid-level south-westerly flow brought very warm, moist and unstable air over Central Europe, creating an environment with high potential instability and therefore conditions favourable to severe thunderstorm development. The first thunderstorms developed during the late evening hours, and the northern Alpine area was affected later that night by severe hailstorms (not shown).

The flow at 700 hPa is south-westerly (Figure 1(a)) and the cold front is detected in the north-western part of the domain over France. The propagation of the front is slow: over the next 2 days, the cold front remains almost stationary. The radar reflectivity pattern indicates a precipitation band with an orientation similar to that of the cold front located approximately 400 km downstream of the cold front. Noticeable is the hail cell that is detected in north-eastern Switzerland at 47.2°N and 8.7°E with a radar reflectivity of ∼60 dBZ.

In Figure 1(b), the same situation is shown at 850 hPa. The cold front is again identified in the western part of the domain but is located slightly more to the east. This can be expected from the characteristic vertical tilt of the front. In addition to the mature cold front, a second front located at the centre of the main reflectivity pattern is identified with strong wind convergence. Such a pre-frontal convergence line is a characteristic that is frequently observed in conjunction with strong pre-frontal thunderstorm activity (Newton, 1950; Rotunno *et al.*, 1988; Meischner *et al.*, 1991; Delden, 1998; Schultz, 2005). From the kinematic perspective of temperature advection, the convergence line is identified as a cold front by our front identification method.

The shape of the frontal areas at 850 hPa is strongly affected by the latent heat released during the formation of cloud droplets. In addition, the 850 hPa surface intersects the ground in many areas, as illustrated in Figure 1(b) by areas with no wind vectors. This underpins the decision to use the fronts as detected at 700 hPa, even though they might be located relatively far from the centre of precipitation. Furthermore, convergence lines are detected more rarely at 700 hPa than at 850 hPa.

For the linkage between hail initiations and approaching cold fronts to be dynamically meaningful, the frontal zone must be located upstream of the hail cell (see Figure 1). Due to the small domain size, all fronts upstream of hail cells are considered in the analysis and no maximum distance criterion is used (the average distance between hail formation and a front is around 200 km; the median distance is 130 km).

3.2. Radar-based hail detection

Radar-based detection of the probability of hail (POH) provides an indirect measure of the occurrence of hail

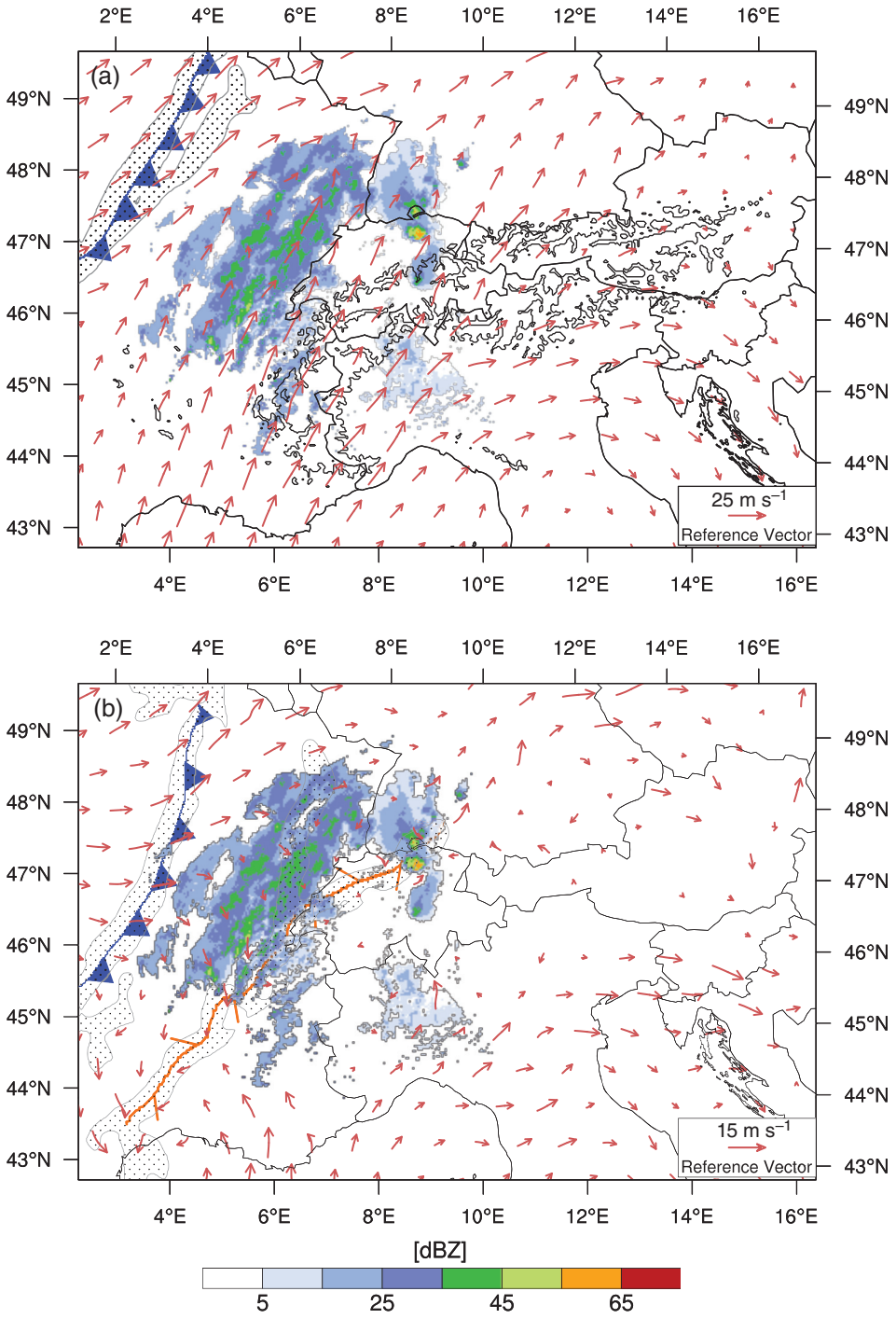

Figure 1. An illustrative example of fronts detected at two different altitudes in COSMO-2 and radar reflectivity at 0600 UTC 1 July 2012. Cold fronts (blue) and wind vectors are shown at (a) 700 hPa and (b) 850 hPa. A pre-frontal convergence line (orange) at 850 hPa aligns with the area of highest reflectivity. Also shown are the frontal zones around each front (stippled lines). Note that the hail cell (~60 dBZ) in north-eastern Switzerland is located on the north-eastern tip of the 850 hPa convergence line. The 1500 m (a.s.l.) topography is also shown in (a).

at the surface. The 3-D radar-based POH statistic of Nisi *et al.* (2016) is based on the difference between the 45-dBZ radar echo top height, i.e. the maximum altitude of the 45-dBZ echo (ET^{45}), and the height of the melting layer (H^0). In this study, H^0 is taken from the COSMO analysis. An empirical relationship, originally derived by Waldvogel *et al.* (1979) from field experiments, relates the height difference between ET^{45} and H^0 in a cloud to the POH. We use the modified empirical relationship proposed by Foote *et al.* (2005), which has been in operational use at MeteoSwiss since 2008. For values below 1.65 km, POH is assumed to be zero. For values greater than 5.8 km, POH is assumed to be 100%. The fit for intermediate values is given following Foote *et al.* (2005). The relationship was used to reprocess POH for the extended hail season over Switzerland for the period between 2002 and 2013. For every 5-min time step, POH is calculated with a

spatial resolution of 1×1 km. Refer to Chapter 3 in the article of Nisi *et al.* (2016) for more details regarding the quality of the hail detection over complex terrain, high-resolution hail statistics and the calibration data. For a detailed description of the Swiss radar network, which consists of three radar stations in western (La Dôle; 6.1°E, 46.4°N; 1680 m a.s.l), north-eastern (Albis; 8.5°E, 47.2°N; 928 m a.s.l) and southern (Monte Lema; 8.8°E, 46.0°N; 1625 m a.s.l.) Switzerland, the reader is referred to the study of Germann *et al.* (2006) and Joss *et al.* (1998). In Figure 2(a), the radar stations are located near Geneva, Zurich and Locarno.

The life cycle of individual thunderstorms and hail cells can be investigated using the radar tracking algorithm Thunderstorm Radar Tracking (TRT) by Hering *et al.* (2004). The underlying criteria for the detection of a convective hail cell in the data set of Nisi *et al.* (2016) are

- a minimum convective cell lifetime of 15 min and
- at least 5 pixels in each cell with POH values greater than 90% for at least 5 min.

A total of 14 000 convective hail cells are identified in the 12-year study period. The locations of hail initiation in the convective cell represent the data base of this study. We henceforth refer to the location of the first detection of a hail signal as the location of hail initiation.

4. Frequency of front detection

Switzerland is commonly affected by eastward propagating synoptic-scale disturbances that are embedded in the mean westerly flow. Cold fronts typically approach Switzerland from the northwest (75%) and only rarely from the southeast (Jenkner *et al.*, 2010). During summer, the largest fraction of fronts that do not propagate into Switzerland from the northwest instead approach the Alps from the southwest (Jenkner *et al.*, 2010). The Alps strongly affect the speed and direction of travel. The distortion of the flow field leads to the slowing and deformation of the fronts (Davies, 1984; Schumann, 1987).

In this section, the frequencies of cold fronts with two different minimum lengths are discussed. The climatology is presented in terms of an occurrence rate (%) of the frontal zones at every gridpoint, which is obtained by a time average of binary frontal fields. To obtain this average, gridpoints containing fronts are labelled with a one; those without are labelled with a zero. A time average over all time steps results in a front frequency. The results presented here show the entire COSMO-2 domain; in all later sections, only a sub-domain around Switzerland is shown to account for the decrease in the quality of radar detection.

The detection frequencies of fronts with minimum lengths of 500 km are shown in Figure 2(a). The obtained frontal frequency highlights regions where fronts typically slow down or become stationary, i.e. upstream of mountain crests, before they become deformed or split. Fronts are frequently identified upstream of the main Alpine ridge (up to ∼6%, Figure 2(a)), as well as upstream of the Jura Mountains in north-western Switzerland (∼4%) and on the southern side of the Alps (∼5%). The detection rates decrease towards the boundaries of the domain due to the fact that fronts that have just entered the domain or are leaving the domain do not fulfil the length criterion.

The front frequencies for fronts with a minimum length of 300 km (Figure 2(b)) show higher detection rates over the Alpine foothills (∼13%). This can be explained by a type of quasi-stationary front that is mainly due to diurnal circulations and that is less frequently detected with the 500 km length criterion. For example, a strong increase in frontal detection rates is found in the south-western part of the Alps, forming a bow-shaped pattern that extends southward towards the Mediterranean, that is much less pronounced in Figure 2(a). This finding agrees with the results of Jenkner *et al.* (2010) and their climatology of meso-scale fronts. They find enhanced detection rates of thermally induced meso-scale fronts along the border between France and Italy, along the upper Rhône Valley and along the French Alps towards the Mediterranean coastline. These fronts are mainly driven by the diurnal evolution of the planetary boundary layer in this region. Moreover, Jenkner *et al.* (2010) point out the pronounced effect of the thermal circulation on the detection of meso-scale fronts along the Mediterranean coastline. In this area, sea breezes contribute to the break up of the inversion layer and can hence assist the growth of localized thermal fronts (Bastin *et al.*, 2005). From the kinematic perspective, these fronts may, according to Equation (2), be classified as cold fronts and hence become part of our front data set, if they also meet the minimum length criterion of 300 km. Based on these results, we decided to require the cold fronts in this study to have a minimum length of 500 km.

5. Statistics of pre-frontal hail formation

Turning to the fraction of pre-frontal hail initiations, a spatially smoothed hail cell initiation statistic is presented in Figure 3(a). The southern parts of Switzerland and the southern Prealps, i.e. the Alpine foothills, are hail initiation hotspots (Figure 3(a); see Punge *et al.*, 2014; Mohr *et al.*, 2015). North of the Alps, western Switzerland, especially along the Jura mountains and the pre-Alpine areas south of Bern, shows an increased occurrence of hail cell initiations. The hotspot region in south-western Germany is a well-known area of frequent thunderstorm activity (Kunz and Puskeiler, 2010). Note that areas of high topography (>1500 m a.s.l.), where the total number of detected hail cells is low, are masked. A more detailed discussion can be found in the study of Nisi *et al.* (2016).

Figure 3(b) presents the relative percentage of all hail initiations occurring downstream of a synoptic-scale

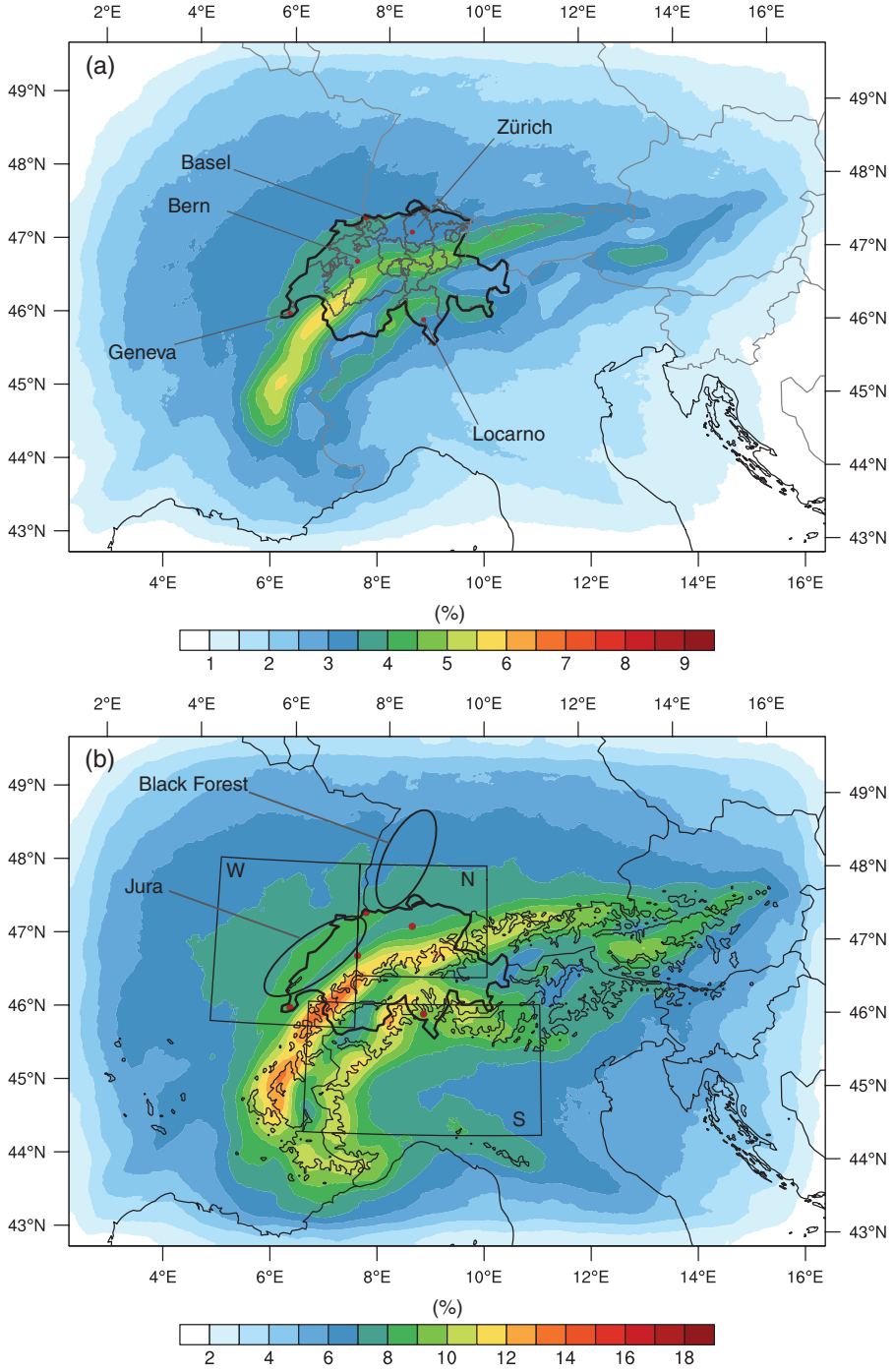

Figure 2. Detection rates of frontal zones with colds fronts with minimum lengths of (a) 500 km and (b) 300 km for the period between 2002–2013 (May to September). The entire COSMO-2 domain is shown, as well as (a) the Swiss administrative areas and five major cities and (b) the 1500 m COSMO-2 model topography (a.s.l).

cold front, i.e. the frontal gridpoint nearest to the hail initiation must be located to its west. Due to the limited domain size, all hail initiations downstream of a cold front are taken into account and no maximum distance limit is set. In the region upstream (windward side) of the Jura Mountains, we find that up to 40–45% of all hail initiations are associated with a cold front to their west. In the Jura Mountains, however, where a high fraction of pre-frontal hail formations are found upstream, a local minimum is identified (<20%). This dipole pattern around an orographic obstacle is also found in south-western Germany, where a minimum in the pre-frontal hail fraction is identified over the Black Forest (<25%) and 30–40% of all pre-frontal hail initiations are formed to the west of the Rhine valley. In north-eastern Switzerland, around Basel and Zurich, more hail initiations are associated with fronts (30–40%) as compared to western Switzerland (20–30%). In western Switzerland, hail formation is frequently due to air mass convection in south-westerly flow situations (Nisi *et al.*, 2016). For southern Switzerland, we identify fronts in up to

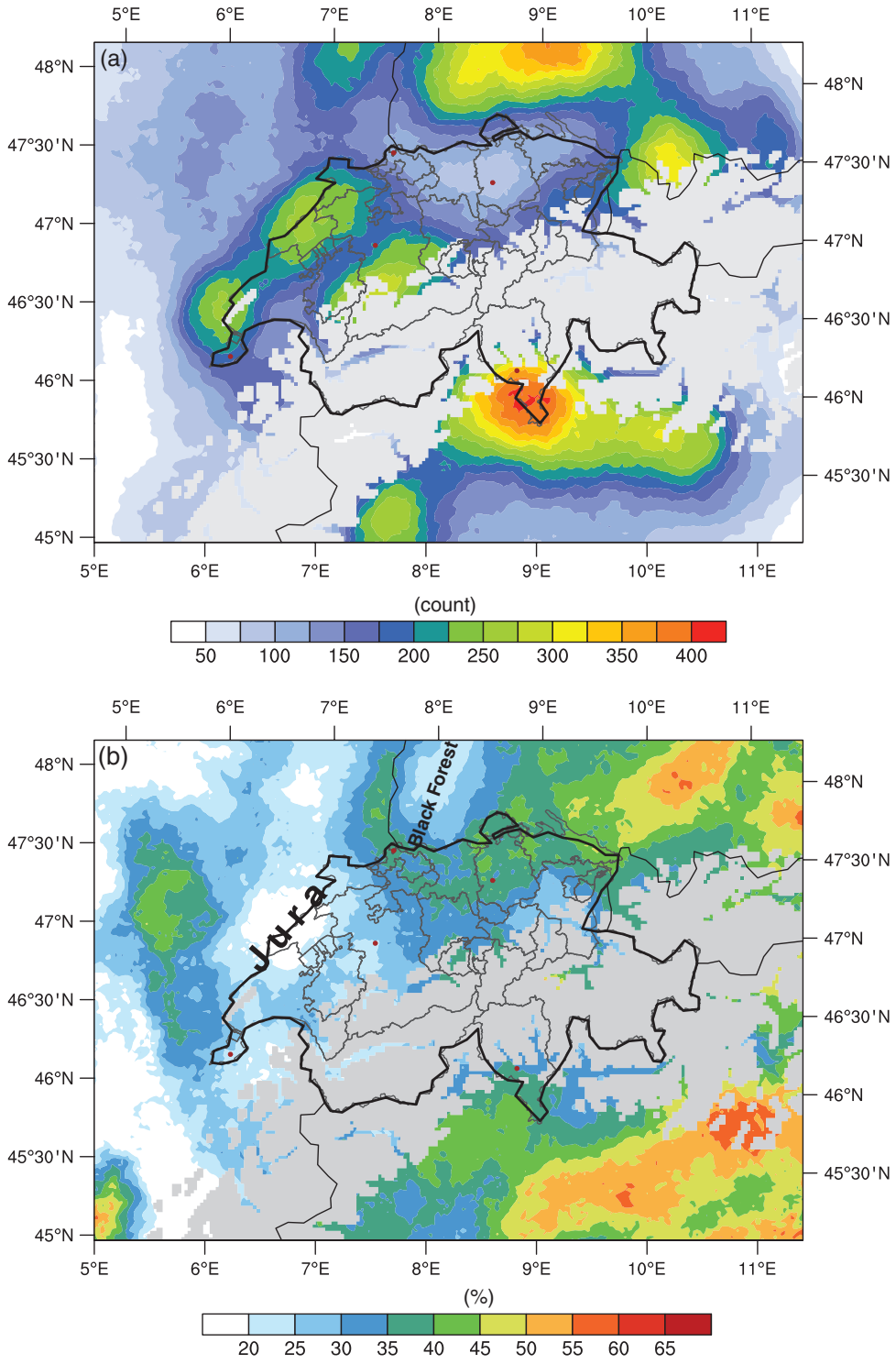

Figure 3. Shown is (a) the smoothed geographical distribution of detected hail cell initiations between 2002 and 2013 (May and September) and (b) the relative fraction of events with a synoptic-scale cold front located to the west. Regions above 1500 m (a.s.l) are masked. The Jura and Black Forest sub-Alpine mountains are labelled.

40% of all hail cases. Although there appears to be a west–east gradient in the percentage of hail initiations with associated synoptic-scale fronts, the local variability over the domain suggests that the eastward increase is not due to the influence of the limited domain size. Although hail occurs statistically less frequently in pre-frontal zones, these findings suggest that hail occurs primarily in pre-frontal zones, with the exception of Ticino on the southern side of the Alps (see Figure 3(a) and (b)).

6. Vertical shear during pre-frontal hail formation

So far, we have focused on the statistical relationship between fronts and the formation of hail. In the

following section, we touch briefly on the potential physical mechanisms that make fronts a key ingredient for the formation of hail cells. One such mechanism is wind shear, which is known to be a crucial factor for long-lived convective cells.

Shear is able to extend the lifetime of a convective cell and multiple-cell storms are likely to occur in a wind-sheared environment. Klemp and Wilhelmson (1978) and Wilhelmson and Klemp (1978) show that convective cells decay if the cold pool at the front of the cell moves away at an early stage. In this case, moist warm air is no longer lifted at the leading edge of the cold pool above the pool and into the cloud. If there is sufficient vertical wind shear; however, the cold pool remains below the convective cell and adds to the vertical lifting of warm air because horizontal vorticity generated at the leading edges of the cold pool forces vertical motion in combination with horizontal ambient vorticity of the opposite sign (Knupp and Cotton, 1982; Rotunno and Klemp, 1985; Rotunno *et al.*, 1988; Weisman *et al.*, 1988; Weisman and Rotunno, 2004; Schlemmer and Hohenegger, 2014) or due to buoyancy forcing by evaporation at the cold pool boundaries (Khairoutdinov and Randall, 2006; Böing *et al.*, 2012; Torris *et al.*, 2015). These mechanical and thermodynamic cold-pool dynamics can also trigger the formation of multiple storm cells (Markowski and Richardson, 2010). Furthermore, Droegemeier and Wilhelmson (1985a) and Droegemeier and Wilhelmson (1985b) describe the collision of two cold pools as driving mechanism behind long-lived convective clouds. For further details, the reader is referred to the study of Markowski and Richardson (2010). Following the arguments presented by Emanuel (1994), the decay of a convective cell is forced at a later stage by the cold pool if updrafts become too weak to lift the cold and dense air into cloud. However, vertical wind shear leads to the formation of non-hydrostatic pressure anomalies, which are a surrogate for positive buoyancy or heating anomalies inside the convective cell. Accordingly, the forcing by the cold pool is offset and the lifetime of the convective cell is extended.

Here we focus on the bulk shear of the meridional wind component (Figure 4). The shear is often measured between 0–6 km (Weisman and Klemp, 1982; Doswell and Evans, 2003; Haklander and Delden, 2003; Groenemeijer and Delden, 2007; Kaltenboeck and Steinheimer, 2015), but because our focus lies not on the actual quantification of the forced lifting but rather on a qualitative assessment of the shear conditions in a broader pre-frontal zone, we consider 700 hPa (which is the pressure level at which fronts are identified) and the 850 hPa level. In the *semi-geostrophic* approximation, the thermal wind balance implies a vertical wind shear of the *along-frontal* wind component proportional to the *across-frontal* temperature gradient (Holton, 2004). If we consider a broader zone around the frontal lines (±500 km) that encompasses the pre-frontal and post-frontal areas, we may argue that the geostrophic approximation is also justified. In the *geostrophic* case, thermal wind balance implies a vertical wind shear of the *meridional* wind component proportional to the *zonal* temperature gradient, i.e. for a hypothetical cold front strictly oriented north–south, it implies a positive vertical shear of the meridional wind component:

$$v_T = v\left(p_1\right) - v\left(p_0\right) = \frac{R}{f} \ln\left(\frac{p_0}{p_1}\right)\left(\frac{\partial \overline{T}}{\partial x}\right)_p . \quad (3)$$

where p_0 is set to 850 hPa, p_1 is set to 700 hPa and $\overline{T}$ denotes the average layer temperature between the two limits (f is the Coriolis parameter and R is the gas constant for dry air). The temporal evolution of the shear is likely driven by the approaching cold fronts.

Figure 4 shows the temporal evolution of the vertical shear of the meridional wind at every hail site. The temporal evolution of the shear is calculated at every location where a hail initiation is detected by the radar. Afterwards we average over all time series with hail initiation in western, north-eastern and southern Switzerland separately. We additionally separate cases in western, north-eastern (northern) and southern Switzerland (domains are shown in Figure 2(b)). However, the vertical shear of the meridional wind increases prior to the first hail initiation in all three domains. In the northern and western sub-domain, this increase is stronger than that in the southern domain, and reaches a maximum 2–4 h before hail formation. Shielding of the fronts by the Alps may be a reason for a weaker shear signal on the southern side of the Alps or a systematically different orientation of the fronts (i.e. more zonally than meridionally oriented). An inspection of the temporal evolution of the distance between the front and the site of hail initiation (not shown) indicates that the increase in shear typically co-occurs with the approaching front. This suggests that one reason why pre-frontal zones are amenable for the formation of long-lived convective cells is because they form a large-scale sheared environment. Further investigations are needed to compare pre-frontal hail cases to front-free cases, but the analysis provides a first indication of the physical mechanisms that contribute to hail formation in pre-frontal zones.

7. Conclusions and summary

The main objective of this study was to investigate the co-occurrence of cold fronts and hail over Switzerland using a large sample (14 000) of hail events for the period between 2002 and 2012 (May–September). To this end, an automated front identification algorithm is applied to a high-resolution regional analysis data set (COSMO-2/-7) covering the Alpine ridge and the front data are linked with radar-based hail signals. Based on this information, we present a statistic of pre-frontal hail initiations.

The front algorithm was successfully adapted to operate on a grid spacing of 2.2 km and performs well in the identification of synoptic-scale cold fronts on 700 hPa.

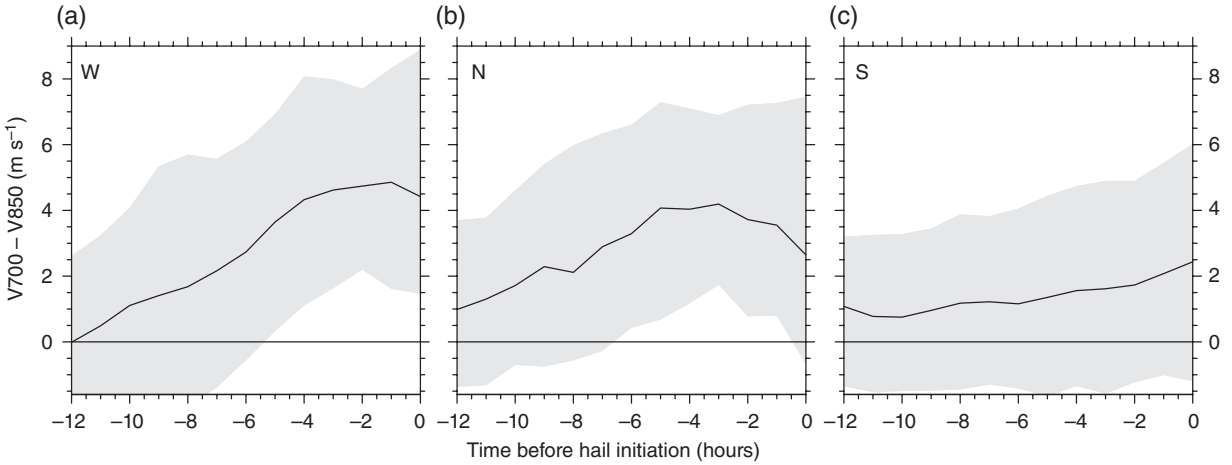

Figure 4. Temporal evolution of meridional bulk wind shear between the 700 and 850 hPa levels (m s^{-1}) prior to hail initiation in (a) western, (b) north-eastern and (c) southern Switzerland. Shown is the median (black) and the interquartile range (25–75% percentile, grey shading).

The obtained 12-year frontal frequencies show maxima in areas where fronts typically become stationary along the Alpine foothills.

We identify regions where the fraction of pre-frontal hail initiations is particularly high. Locally, the fraction increases to up to 40–45%, *particularly in areas where the total number of hail initiations is small*, i.e. in north-eastern Switzerland. This finding suggests that hail initiations in these areas require fronts as an additional agent to force intense convection. Elsewhere orographic forcing is potentially strong enough to provide enough lifting to trigger hail storms. On the southern side of the Alps, the Ticino region is an exception. There, hail occurs frequently and is associated with pre-frontal conditions in 40% of all cases. On average, the distance between the front line and the point of hail initiation is around 200 km, with a median value of ∼130 km.

Finally, we examined the temporal evolution of the vertical shear of the meridional wind (between 850 and 700 hPa) at the sites of hail initiation. We find an increase in shear until around 1 h prior to the detection of hail for cases north of the Alps, and a continued increase for cases south of the Alps (note that the temporal resolution of the data set is 1 h). Because cold fronts are associated with vertical wind shear, and because wind shear is known to be a favourable condition for the formation of long-lived convective cells, we argue that frontal zones are amenable for the formation of hail (among other effects, not discussed in this study; such as along-frontal moisture transport (see Doswell, 2001)).

The obtained data set of pre-frontal hail initiations over Switzerland can be further used to, e.g. directly compare the characteristics of hail cases associated with fronts to cases without fronts and to quantify the role of pre-frontal moisture advection, lifting and destabilization. The data set might also be used to explore the relationship between hail and other significant weather events such as wind gusts or lightning.

Acknowledgements

We would like to thank MeteoSwiss for granting access to the COSMO-2/-7 analysis and radar data set.

References

Alberoni PP, Levizzani V, Watson RJ, Holt AR, Costa S, Mezzasalma P, Nanni S. 2000. The 18 June 1997 companion supercells: multiparametric doppler radar analysis. *Meteorology and Atmospheric Physics* **75**: 101–120, doi: 10.1007/s007030070018.

Allen JT, Karoly DJ. 2014. A climatology of Australian severe thunderstorm environments 1979–2011: inter-annual variability and ENSO influence. *International Journal of Climatology* **34**: 81–97, doi: 10.1002/joc.3667.

Bastin S, Dobrinski P, Dabas A, Delville P, Reitebuch O, Werner C. 2005. Impact of the Rhône and Durance valley on sea-breeze circulation in the Marseille area. *Atmospheric Research* **74**: 303–328, doi: 10.1016/j.atmosres.2004.04.014.

Berry G, Reeder MJ, Jakob C. 2011. A global climatology of atmospheric fronts. *Geophysical Research Letters* **38**: L04809, doi: 10.1029/2010GL046451.

Böing SJ, Jonker JJ, Siebesma AP, Grabowski WW. 2012. Influence of the subcloud layer on the development of a deep convective ensemble. *Journal of the Atmospheric Sciences* **69**: 2682–2698, doi: 10.1175/JAS-D-11-0317.1.

Brooks HE. 2009. Proximity soundings for severe convection for Europe and the United States from reanalysis data. *Atmospheric Research* **93**: 546–553, doi: 10.1016/j.atmosres.2008.10.005.

Brooks HE, Lee JW, Craven JP. 2003. The spatial distribution of severe thunderstorms and tornado environments from global reanalysis data. *Atmospheric Research* **67–68**: 73–94, doi: 10.1016/S0169-8095(03)00045-0.

Costa S, Mezzasalma P, Levizzani V, Alberoni PP, Nanni S. 2001. Deep convection over Northern Italy: synoptic and thermodynamic analysis. *Atmospheric Research* **56**: 73–88, doi: 10.1016/S0169-8095(00)00091-0.

Davies HC. 1984. On the orographic retardation of a cold front. *Contributions to Atmospheric Physics (Beiträge zur Physik der Atmosphäre)* **57**: 409–418.

Davies JM. 2004. Estimations of CIN and LFC associated with tornadic and nontornadic supercells. *Weather and Forecasting* **19**: 714–726.

Delden AV. 1998. The synoptic setting of a thundery low and associated prefrontal squall line in Western Europe. *Meteorology and Atmospheric Physics* **65**: 113–131, doi: 10.1007/BF01030272.

Doswell CA III. 1987. The distinction between large-scale and mesoscale contribution to severe convection: A case study example. *Weather and Forecasting* **2**: 3–16.

Doswell CA III (ed). 2001. *Severe Convection Storms*, Vol. **28**. American Meteorological Society. American Meteorological Society: Boston, MA, 561 pp.

Doswell CA III, Evans JS. 2003. Proximity sounding analysis for derechos and supercells: an assessment of similarities and differences. *Atmospheric Research* **67–68**: 117–133, doi: 10.1016/S0169-8095(03)00047-4.

Droegemeier K, Wilhelmson R. 1985a. Three-dimensional numerical modeling of convection produced by interacting thunderstorm outflows. Part I: control simulation and low-level moisture variations. *Journal of the Atmospheric Sciences* **42**: 2381–2403, doi: 10.1175/1520-0469(1985)042<2381:TDNMOC>2.0.CO;2.

Droegemeier K, Wilhelmson RB. 1985b. Three-dimensional numerical modeling of convection produced by interacting thunderstorm outflows. Part II: variations in vertical wind shear. *Journal of the Atmospheric Sciences* **42**: 2404–2414, doi: 10.1175/1520-0469(1985)042<2404:TDNMOC>2.0.CO;2.

Droegemeier KK, Lazarus SM, Davies-Jones R. 1993. The influence of helicity on numerically-simulated convective storms. *Monthly Weather Review* **121**: 2005–2029.

Emanuel K. 1994. *Atmospheric Convection*. Oxford University Press, Inc.: New York, NY.

Fawbush EJ, Miller RC. 1954. The types of air masses in which North American tornadoes form. *Bulletin of the American Meteorological Society* **35**: 154–165.

Foote G, Krauss TW, Makitov V. 2005. *Hail metrics using convectional radar*. 16th Conference on Planned and Inadvertent Weather Modification. The 85th AMS Annual Meeting: San Diego, CA.

Gensini VA, Mote TL, Brooks HE. 2014. Severe thunderstorm reanalysis environments and collocated radiosonde observations. *Journal of Applied Meteorology and Climatology* **53**: 742–751, doi: 10.1175/JAMC-D-13-0263.1.

Germann U, Galli G, Boscacci M, Bolliger M. 2006. Radar precipitation measurement in a mountainous region. *Quarterly Journal of the Royal Meteorological Society* **132**: 1669–1692, doi: 10.1256/qj.05.190.

Giaiotti D, Nordio S, Stel F. 2003. The climatology of hail in the plain of Friuli Venezia Giulia. *Atmospheric Research* **67–68**: 247–259, doi: 10.1016/S0169-8095(03)00084-X.

Grams JS, Thompson RL, Snively DV, Prentice JA, Hodges GM, Reames LJ. 2012. A climatology and comparison of parameters for significant tornado events in the United States. *Weather and Forecasting* **27**: 106–123, doi: 10.1175/WAF-D-11-00008.1.

Groenemeijer P, Delden AV. 2007. Sounding-derived parameters associated with large hail and tornadoes in the Netherlands. *Atmospheric Research* **83**: 473–487, doi: 10.1016/j.atmosres.2005.08.006.

Haklander AJ, Delden AV. 2003. Thunderstorm predictors and their forecast skill for the Netherlands. *Atmospheric Research* **67–68**: 273–299, doi: 10.1016/S0169-8095(03)00056-5.

Hering AM, Morel C, Galli G, Sénési S, Ambrosetti P, Boscacci M. 2004. Nowcasting thunderstorms in the Alpine region using a radar based adaptive thresholding scheme. 3rd European Conference on Radar in Meteorology and Hydrology, 6–10 September 2004, Visby, Sweden.

Hewson DT. 1998. Objective fronts. *Meteorological Applications* **5**: 37–65, doi: 10.1017/S1350482798000553.

Heymsfield GM, Schotz S. 1985. Structure and evolution of a severe squall line over Oklahoma. *Monthly Weather Review* **113**: 1563–1589.

Holton JR. 2004. *An Introduction to Dynamic Meteorology*, 4 ed. Elsevier Academic Press: London, UK.

Houze RA Jr, Schmid W, Fovell RG, Schiesser HH. 1993. Hailstorms in Switzerland: left movers, right movers, and false hooks. *Monthly Weather Review* **121**: 3345–3370.

Huntrieser H, Schiesser HH, Schmid W, Waldvogel A. 1997. Comparison of traditional and newly developed thunderstorm indices for Switzerland. *Weather and Forecasting* **12**: 108–125, doi: 10.1175/1520-0434(1997)012<0108:COTAND>2.0.CO;2.

Jenkner J, Sprenger M, Schwenk I, Schwierz C, Dierer S, Leuenberger D. 2010. Detection and climatology of fronts in a high-resolution model reanalysis over the Alps. *Meteorological Applications* **17**: 1–18, doi: 10.1002/met.142.

Joss J, Schädler B, Galli G, Cavalli R, Boscacci M, Held E, Bruna GD, Kappenberger G, Nespor V, Spiess R. 1998. *Operational Use of Radar for Precipitation Measurements in Switzerland*, Vol. **134**. Vdf Hochschulverlag AG ETH Zurich: Zuerich, Switzerland, http://www.meteoschweiz.admin.ch/content/dam/meteoswiss/fr/Mess-und-Prognosesysteme/doc/meteoswiss_operational_use_of_radar.pdf.

Kaltenboeck R, Steinheimer M. 2015. Radar-based severe storm climatology for Austrian complex orography related to vertical wind shear and atmospheric instability. *Atmospheric Research* **158–159**: 216–230, doi: 10.1016/j.atmosres.2014.08.006.

Khairoutdinov FM, Randall D. 2006. High-resolution simulation of shallow-to-deep convection transition over land. *Journal of the Atmospheric Sciences* **63**: 3421–3436, doi: 10.1175/Jas3810.1.

Klemp JB, Wilhelmson RB. 1978. The simulation of three-dimensional convective storm dynamics. *Journal of the Atmospheric Sciences* **35**: 1070–1096, doi: 10.1175/1520-0469(1978)035<1070:TSOTDC>2.0.CO;2.

Knupp K, Cotton W. 1982. An intense, quasi-steady thunderstorm over mountainous terrain. Part II: doppler radar observations of the storm morphological structure. *Journal of the Atmospheric Sciences* **39**: 343–358, doi: 10.1175/1520-0469(1982)039<0343:AIQSTO>2.0.CO;2.

Kunz M, Puskeiler M. 2010. High-resolution assessment of the hail hazard over complex terrain from radar and insurance data. *Meteorologische Zeitschrift* **10**: 427–439, doi: 10.1127/0941-2948/2010/0452.

Locatelli JD, Martin JE, Castle JA, Hobbs PV. 1995. Structure and evolution of winter cyclones in the Central United States and their effects on the distribution of precipitation. Part III: the development of a squall line associated with weak cold frontogenesis aloft. *Monthly Weather Review* **123**: 2641–2662.

Manzato A. 2012. Hail in northeast Italy: climatology and bivariate analysis with the sounding-derived indices. *Journal of Applied Meteorology and Climatology* **51**: 449–467, doi: 10.1175/JAMC-D-10-05012.1.

Manzato A. 2013. Hail in northeast Italy: a neural network ensemble forecast using sounding-derived indices. *Weather and Forecasting* **28**: 3–28, doi: 10.1175/WAF-D-12-00034.1.

Markowski P, Richardson Y. 2010. *Mesoscale Meteorology in Midlatitudes*. John Wiley & Sons: West Sussex, UK, doi: 10.1002/9780470682104.

Meischner PF, Bringi VN, Heimann D, Höller H. 1991. A squall line in southern Germany: kinematics and precipitation formation as deduced by advanced polarimetric and doppler radar measurements. *Monthly Weather Review* **119**: 678–701, doi: 10.1175/1520-0493(1991)119<0678:ASLISG>2.0.CO;2.

Merino A, Wu X, Gascón E, Berthet C, Garca-Ortega E, Dessens J. 2014. Hailstorms in southwestern France: incidence and atmospheric characterization. *Atmospheric Research* **140–141**: 61–75, doi: 10.1016/j.atmosres.2014.01.015.

Mohr S, Kunz M. 2013. Trend analysis of convective indices relevant for hail events in Germany and Central Europe. *Atmospheric Research* **123**: 211–228, doi: 10.1016/j.atmosres.2012.05.016.

Mohr S, Kunz M, Geyer B. 2015. Hail potential in Europe based on a regional climate model hindcast. *Geophysical Research Letters* **42**: 10,904–10,912, doi: 10.1002/2015GL067118.

Naylor J, Gilmore MS. 2012. Environmental factors influential to the duration and intensity of tornadoes in simulated supercells. *Geophysical Research Letters* **39**(L17): 802, doi: 10.1029/2012GL053041.

Neiman PJ, Wakimoto RM. 1999. The interaction of a pacific cold front with shallow air masses east of the Rocky Mountains. *Monthly Weather Review* **127**: 2102–2127.

Newton CW. 1950. Structure and mechansim of the prefrontal squall line. *Journal of Meteorology* **7**: 210–222, doi: 10.1175/1520-0469(1950)007<0210:SAMOTP>2.0.CO;2.

Nisi L, Martius O, Hering A, Germann U. 2016. Spatial and temporal distribution of hailstorm in the Alpine region: a long-term, high resolution, radar-based analysis. *Quarterly Journal of the Royal Meteorological Society*, doi: 10.1002/qj.2771.

Ogura Y, Portis D. 1982. Structure of the cold front observed in SESAME-AVE III and its comparison with the Hoskins-Bretherton

frontogenesis model. *Journal of the Atmospheric Sciences* **39**: 2773–2792, doi: 10.1175/1520-0469(1982)039<2773:SOTCFO>2.0.CO;2.

Punge HJ, Bedka KM, Kunz M, Werner A. 2014. A new physically based stochastic event catalog for hail in Europe. *Natural Hazards* **73**: 1625–1645, doi: 10.1007/s11069-014-1161-0.

Rasmussen EN, Blanchard DO. 1998. A baseline climatology of sounding-derived supercell and tornado forecast parameters. *Weather and Forecasting* **13**: 1148–1164, doi: 10.1175/1520-0434(1998)013<1148:ABCOSD>2.0.CO;2.

Renard R, Clarke L. 1965. Experiments in numerical objective frontal analysis. *Monthly Weather Review* **93**: 547–556, doi: 10.1175/1520-0493(1965)093<0547:EINOFA>2.3.CO;2.

Rotunno R, Klemp J. 1985. On the rotation and propagation of simulated supercell thunderstorms. *Journal of the Atmospheric Sciences* **42**: 271–292, doi: 10.1175/1520-0469(1985)042<0271:OTRAPO>2.0.CO;2.

Rotunno R, Klemp JB, Weisman ML. 1988. A theory for strong, long-lived squall lines. *Journal of the Atmospheric Sciences* **45**: 463–485, doi: 10.1175/1520-0469(1988)045<0463:ATFSLL>2.0.CO;2.

Schemm S, Sprenger M. 2015. Frontal-wave cyclogenesis in the North Atlantic – a climatological characterisation. *Quarterly Journal of the Royal Meteorological Society* **141**: 2989–3005, doi: 10.1002/qj.2584.

Schemm S, Rudeva I, Simmonds I. 2015. Extratropical fronts in the lower troposphere – global perspectives obtained from two automated methods. *Quarterly Journal of the Royal Meteorological Society* **141**: 1686–1698, doi: 10.1002/qj.2471.

Schiesser HH, Waldvogel A, Schmid W, Willemse S. 1997. *Klimatologie der Stürme und Sturmsysteme anhand von Radar - und Schadendaten (in German)*, Vol. **132**. Vdf Hochschulverlag AG ETH Zurich: Zuerich, Switzerland.

Schlemmer L, Hohenegger C. 2014. The formation of wider and deeper clouds as a result of cold-pool dynamics. *Journal of the Atmospheric Sciences* **71**: 2842–2858, doi: 10.1175/JAS-D-13-0170.1.

Schultz DM. 2005. A review of cold fronts with prefrontal troughs and wind shifts. *Monthly Weather Review* **133**: 2449–2472, doi: 10.1175/MWR2987.1.

Schumann U. 1987. Influence of mesoscale orography on idealized cold fronts. *Journal of the Atmospheric Sciences* **44**: 3423–3441, doi: 10.1175/1520-0469(1987)044<3423:IOMOOI>2.0.CO;2.

Steppler JG, Doms G, Schättler U, Bitzer HW, Gassmann A, Damrath U, Gregoric G. 2003. Meso-gamma scale forecasts using the non-hydrostatic model LM. *Meteorology and Atmospheric Physics* **82**: 75–96, doi: 10.1007/s00703-001-0592-9.

Suwala K, Bednorz E. 2013. Climatology of hail in central Europe. *Quaestiones Geographicae* **32**: 99–110, doi: 10.2478/quageo-2013-0025.

Torris G, Kuang Z, Tian Y. 2015. Mechanisms for convection triggering by cold pools. *Geophysical Research Letters* **42**: 1943–1950, doi: 10.1002/2015GL063227.

Towery NG, Changnon SA. 1970. Characteristics of hail-producing radar echoes in Illinois. *Monthly Weather Review* **98**: 346–353, doi: 10.1175/1520-0493(1970)098<0346:COHPRE>2.3.CO;2.

Waldvogel A, Federer B, Grimm P. 1979. Criteria for the detection of hail cells. *Journal of Applied Meteorology and Climatology* **18**: 1521–1525, doi: 10.1175/1520-0450(1979)018<1521:CFTDOH>2.0.CO;2.

Weisman ML, Klemp JB. 1982. The dependence of numerically simulated convective storms on vertical wind shear and buoyancy. *Monthly Weather Review* **110**: 504–520, doi: 10.1175/1520-0493(1982)110<0504:TDONSC>2.0.CO;2.

Weisman M, Rotunno R. 2004. "A theory for strong, long-lived squall lines" revisited. *Journal of the Atmospheric Sciences* **61**: 361–382.

Weisman M, Klemp J, Rotunno R. 1988. Structure and evolution of numerically simulated squall lines. *Journal of the Atmospheric Sciences* **45**: 1990–2013, doi: 10.1175/1520-0469(1988)045<1990:SAEONS>2.0.CO;2.

Weissmann M, Braun F, Ganter L, Mayr G, Rahm S, Reitebuch O. 2005. The Alpine mountain-plain circulation: Airborne doppler lidar measurements and numerical simulations. *Monthly Weather Review* **133**: 3095–3109, doi: 10.1175/MWR3012.1.

Wilhelmson RB, Klemp JB. 1978. A numerical study of storm splitting that leads to long-lived storms. *Journal of the Atmospheric Sciences* **35**: 1974–1986, doi: 10.1175/1520-0469(1978)035<1974:ANSOSS>2.0.CO;2.

Willemse S. 1995. A statistical analysis and climatological interpretation of hailstorms in Switzerland. PhD thesis, ETH, Zurich, Switzerland, 10.3929/ethz-a-001486581.